JACS
JOURNAL OF THE AMERICAN CHEMICAL SOCIETY
Article
pubs.acs.org/JACS

# Unusual High-Temperature Reversible Phase-Transition Behavior, Structures, and Dielectric–Ferroelectric Properties of Two New Crown Ether Clathrates

Yun-Zhi Tang,* Yin-Mei Yu, Jian-Bo Xiong, Yu-Hui Tan, and He-Rui Wen

School of Metallurgy and Chemical Engineering, Jiangxi University of Science and Technology, Ganzhou 341000, PR China

Supporting Information

**ABSTRACT:** Molecular ferroelectrics with high-temperature reversible phase-transition behaviors are very rare and have currently become one of the hotspots in the field of ferroelectric materials. Herein we display two new crown ether clathrates possessing unusual high-temperature ferroelectric phase-transition behaviors, cyclohexyl ammonium 18-crown-6 tetrafluoroborate (or perchlorate), $[Hcha\text{-}(18\text{-crown-}6)]^+$ $[BF_4]^-$ (**1**) and $[Hcha\text{-}(18\text{-crown-}6)]^+[ClO_4]^-$ (**2**) (Hcha = protonated cyclohexyl ammonium). We have proven their reversible structural phase transitions by variable-temperature PXRD measurements and temperature evolutions of Raman bands. Both clathrates exhibit clear ferroelectric phase transitions at about 397 and 390 K, respectively, revealed by the thermal anomalies of differential scanning calorimetry (DSC) measurements, together with abrupt dielectric anomalies in the heating and cooling processes. The measurements on ferroelectric properties using the single crystals showed optimized spontaneous polarization ($P_s$) of ca. 3.27 $\mu$C cm$^{-2}$ for **1** and 3.78 $\mu$C cm$^{-2}$ for **2**.

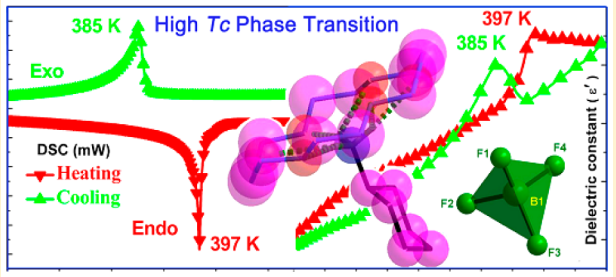


## 1. INTRODUCTION

As a kind of multifunctional electroactive materials, ferroelectrics have found a range of applications in modern memory elements, filtering devices, and high-performance insulators.[1−4] In recent years, research on ferroelectric materials based on metal−organic frameworks (MOFs) and organic salts have received considerable attention in the new round of molecular materials[5,6] because they are promising with obvious advantages such as light weight, structural diversity, mechanical flexibility, and lead-free environmentally friendly processing. However, to the best of our knowledge, there exist a lot of difficulties in exploring new types of molecular ferroelectrics as follows:[7,8] (i) Most known molecular ferroelectrics such as organic salts and MOFs have low phase-transition temperatures (Curie temperature, $T_c$), usually below room temperature, and small spontaneous polarization ($P_s$), which makes them difficult to use in applications of modern ferroelectric materials. (ii) The structures of most molecular compounds are often seriously disordered when the phase-transition temperature is higher than 373 K; thus, the characterization and analysis of their crystal structures to clarify the mechanism of polarization will become a new challenge. (iii) There are still some traditional difficulties in researching a new type of ferroelectrics because they must meet the basic conditions such as undergoing a reversible structural phase transition, belonging to one of the 10 polar point groups in ferroelectric phases (1, *m*, 2, *mm*2, 3, 3*m*, 4, 4*mm*, 6, and 6*mm*), and possessing standard dielectric hysteresis loops.

In our previous works, we have discovered that the protonated organic amine $R{-}NH_3^+$ cation (R = organic groups) can be easily anchored in the cavity of 18-crown-6 and act as a rotator or pendulator in the molecular machine design. Such interactions can create an effective structural polarization, which affords a new way to explore the molecular ferroelectricity. By using this method, some new ferroelectric crown ether clathrates, such as 4-methoxyanilinium 18-crown-6 tetrafluoroborate ($[C_7H_{10}NO\text{-}(18\text{-crown-}6)]^+[BF_4]^-$) and $[(DIPA)(18\text{-crown-}6)]BF_4$ (DIPA = 2,6-diisopropylanilinium) were synthesized with large dielectric anomalies at low temperature (127 and 120 K, respectively).[9,10] These studies clearly show that different organic amines and even different anions have a great impact on their phase-transition temperatures and polarization intensity.

As a systematic investigation of molecular ferroelectrics, we tried to construct and seek out some new types of clathrate compounds with reversible phase-transition behaviors by assembling different organic amines and anions with 18-crown-6. We found interesting new clathrate compounds of 18-crown-6 with cyclohexyl ammonium tetrafluoroborate (or perchlorate) ($[Hcha\text{-}(18\text{-crown-}6)]^+[BF_4]^-$, **1** and $[Hcha\text{-}(18\text{-crown-}6)]^+[ClO_4]^-$, **2**, respectively). They display unusual high ferroelectric phase-transition temperatures at 397 K for **1** and 390 K for **2**, respectively, and large spontaneous polarization ($P_s$) of ca. 3.78 and 3.27 $\mu$C/cm$^2$, respectively. Significantly,

**Received:** July 31, 2015
**Published:** September 28, 2015





DOI: 10.1021/jacs.5b08061
J. Am. Chem. Soc. 2015, 137, 13345−13351

although these compounds may be seriously disordered at high temperature and X-ray single-crystal diffraction is not available, variable-temperature PXRD measurements and temperature evolutions of Raman bands here can become a useful way to explain the local microstructural changes of the reversible structural phase transitions. Herein we detail their reversible structural phase transitions by X-ray powder diffraction, Raman spectra, and apparent reversible anomalies of dielectric and heat as well as their clear, perfect dielectric hysteresis loops.

## 2. EXPERIMENTAL SECTION

**2.1. Synthesis.** As illustrated in Scheme 1, compound **1** was obtained by slow evaporation of a solution of mixed methanol and chloroform ($V_{methanol}/V_{chloroform}$ = 10:1) containing cyclohexylammine, tetrafluoroborate acid, and 18-crown-6 in a 1:1:1 molar ratio. The colorless large block crystals were obtained with a yield of about 77% based on cha after a few days (Figure S1). Anal. Found (Calcd) for $C_{18}H_{38}BF_4NO_6$: C, 47.8 (47.9); H, 8.4 (8.4); N, 3.2 (3.1). IR ($cm^{-1}$) 3150 (m), 2915 (m), 1612 (m), 1535 (s), 1464 (s), 1383 (m), 1286 (m), 1105 (s), 1055 (s), 958 (s), 834 (m), 524 (m). Compound **2** was synthesized with a yield of about 75% by the same manipulations but using perchloric acid instead of tetrafluoroboric acid (Figure S1). Anal. Found (Calcd) for $C_{18}H_{38}ClNO_{10}$: C, 46.6 (46.5); H, 8.1 (8.2); N, 2.9 (3.0). IR ($cm^{-1}$) 3148 (m), 2916 (m), 1610 (m), 1533 (s), 1457 (s), 1379 (m), 1285 (m), 1092 (s), 955 (s), 767 (m), 621 (m), 524 (m).

**Scheme 1. Preparation of the Crown Ether Clathrates**[a]

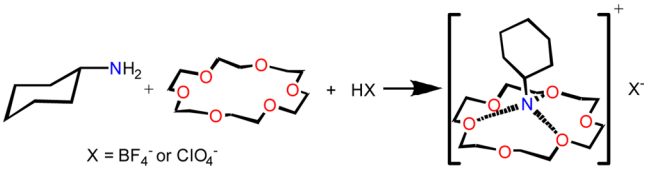


[a] $X^-$ = $BF_4^-$ for **1** and $ClO_4^-$ for **2**.

**2.2. Single-Crystal X-ray Crystallography.** X-ray diffraction experiments were carried out on **1** and **2** using a Rigaku Saturn 924 diffractometer with Mo K$\alpha$ radiation ($\lambda$ = 0.71073 Å) at room temperature and high temperatures (above their transition temperatures). All the treatment including data collection, cell refinement, and data reduction were conducted by using the CrystalClear software package (Rigaku). The structures were resolved by direct methods and refined by the full-matrix method based on $F^2$ using the SHELXTL software package.[11] All non-hydrogen atoms were refined anisotropically, and all hydrogen atoms were generated geometrically. Crystal data for **1** at 293 K: $C_{18}$ $H_{38}BF_4NO_6$, colorless, 0.20 × 0.18 × 0.16 $mm^3$, $M_r$ = 451.30, orthorhombic, $Pca2_1$, $a$ = 13.381(3) Å, $b$ = 12.051(2) Å, $c$ = 14.234(3) Å, $V$ = 2295.3(8) $Å^3$, $Z$ = 4, $D_{calc}$ = 1.306 $g/cm^3$, $\mu$ = 0.115 $mm^{-1}$, $S$ = 1.058, $R(F)$ = 0.0706, $wR(F^2)$ = 0.1923. Crystal data for **2** at T = 293(2) K: $C_{18}$ $H_{38}ClNO_{10}$, colorless, 0.22 × 0.20 × 0.18 $mm^3$, $M_r$ = 464.94, orthorhombic, $Pca2(1)$, $a$ = 13.2727(6) Å, $b$ = 12.2599(6) Å, $c$ = 14.2024(6) Å, $V$ = 2311.04 (18) $Å^3$, $Z$ = 4, $D_{calc}$ = 1.333 $g/cm^3$, $\mu$ = 0.217 $mm^{-1}$, $S$ = 1.024, $R(F)$ = 0.0464, $wR(F^2)$ = 0.1162. These data can be obtained free of charge from the Cambridge Crystallographic Data Centre via http://www.ccdc.cam.ac.uk/data_request/cif. (CCDC nos. 1413963 for **1** and 1007512 for **2**.)

**2.3. Measurement Methods.** Infrared (IR) spectra were recorded on a Shimadzu IRPrestige-21. Powder X-ray diffraction (PXRD) data was recorded on a Rigaku D/MAX 2000 PC X-ray diffraction instrument. The temperature evolution of the Raman spectra of **1** and **2** was carried out in the 180° backscattering geometry, using a 532 nm excitation from a diode-pumped frequency-doubled Nd:YAG solid-state laser (model GDLM-5015 L, Photop Suwtech Inc., China) and a custom-built Raman spectrometer equipped with a SPEX TRIAX 550 monochromator and a liquid-nitrogen-cooled CCD (Spectrum One with CCD 3000 controller, ISA Jobin Yovn).

DSC measurements were conducted with a PerkinElmer Diamond DSC under nitrogen atmosphere with a heating or cooling rate of 5 K/min. Detailed heat analyses were treated on a Quantum Design PPMS. Above-room-temperature thermogravimetric analysis (TGA) measurements were recorded using a TA-Instruments STD 2960 from 293 to 1000 K.

Dielectric measurements were carried out with the single crystals. Silver conduction paste deposited on both surfaces was used as the electrodes. The compounds' dielectric constants were determined with an Agilent or a TH2828A impedance analyzer over the frequency range of 1 kHz to 1 MHz. Their ferroelectric properties were measured by single crystals using a standard RT 6000 ferroelectric tester (Radiant Technologies, Alberquerque, USA) at variable temperature. When samples were immerged in insulating oil, the electric hysteresis loop was observed by Virtual Ground Mode. (The measurement is alternating current; the frequency is 5−50 Hz.)

## 3. RESULTS AND DISCUSSION

**3.1. Crystal Structure Discussions.** At room temperature (293 K), compound **1** belongs to an orthorhombic space group $Pca2_1$ (point group $mm2$), which is noncentrosymmetric and polar. As shown in Figure 1a, the asymmetric unit of **1** is composed of one $[Hcha\text{-}(18\text{-crown-}6)]^+$ complex cation and one $BF_4^-$ anion. The protonated cyclohexyl ammonium cation makes N−H···O hydrogen bonds to 18-crown-6, forming the

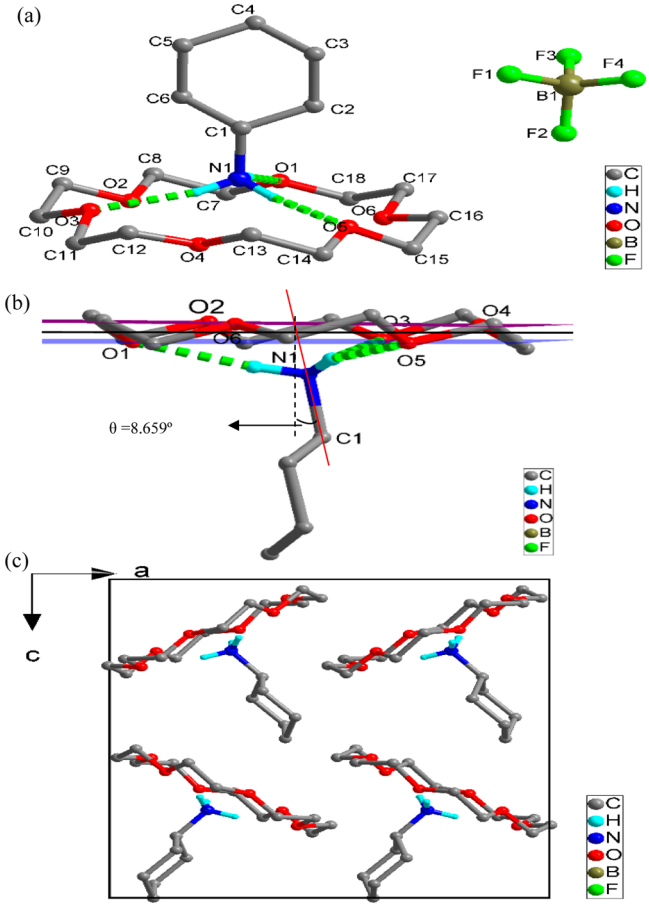


**Figure 1.** (a) Asymmetric unit of compound **1**. (b) Representation of the supramolecular cation, showing the upper plane (purple), mean plane (dark) and lower plane (blue) as well as the torsion angle. (c) Packing view along the $b$ axis.



DOI: 10.1021/jacs.5b08061
J. Am. Chem. Soc. 2015, 137, 13345−13351

crown ether clathrate. As expected, the cyclohexyl group adopts a stable "chair" conformation to reduce torsion strain in the structure, and the whole 18-crown-6 macrocycle is close to an ideal crown formation $D_{3d}$.[9,10] Correspondingly, half of the oxygen atoms of the 18-crown-6 including O1, O3, and O5 atoms are distinctly located below the median plane of the ring (0.2276, 0.2382, and 0.1972 Å, respectively), whereas others (O2, O4, and O6 atoms) are above the plane (0.2149, 0.1973, and 0.1908 Å, respectively). This can be further confirmed by their hydrogen bond lengths (Figure 1a and Table 1). The

**Table 1. Intermolecular Hydrogen Bond Lengths (Å) and Angles (Degrees) for 1 and 2**

| D−H···A | D−H | H···A | D···A | ∠D−H···A |
|---|---|---|---|---|
| | | **1** | | |
| N1−H1A···O1 | 0.89 | 2.03 | 2.915(4) | 171.0 |
| N1−H1B···O3 | 0.89 | 2.04 | 2.920(4) | 164.1 |
| N1−H1C···O5 | 0.89 | 2.07 | 2.933(4) | 169.7 |
| | | **2** | | |
| N1−H1A···O2 | 0.89 | 2.05 | 2.914(3) | 164.2 |
| N1−H1B···O4 | 0.89 | 2.03 | 2.912(3) | 169.6 |
| N1−H1C···O6 | 0.89 | 2.02 | 2.905(3) | 171.6 |

lengths of hydrogen bonds between the hydrogen donor N1 and the hydrogen acceptors O1, O3, and O5 are 2.915(4), 2.933(4), and 2.921(4) Å, respectively, somewhat shorter than those of the other three between N1 and O2, O4, and O6) (3.040(4), 2.980(4), and 3.036(4) Å, respectively). Similar to that in our previous reported crown ether clathrates, the N atom of the cyclohexylammonium cation is located at a position of 0.9680 Å above the best plane of the oxygen atoms in the crown ring, instead of lying in the nesting position of crown ring. In addition, as illustrated in Figure 1b, a torsion angle with a value of 8.659(159) between the N1−C1 bond and the line normal to the best plane can be clearly seen.

Similar to that in compound **1**, some of the oxygen atoms (O1, O3, and O5) in compound **2** are also located above the mean O atom plane with distances of 0.2451, 0.2022, and 0.2128 Å, respectively, whereas the other oxygen atoms (O2, O4, and O6) are located below the median plane of the ring with distances of 0.1936, 0.2090, and 0.2157 Å, respectively (Figures S2 and S3). The amino group of the Hcha cations are firmly attached to the oxygen atoms of the crown ring in a perching way through the strong intermolecular hydrogen bonds (N1−H1A···O2, 2.914(3) Å, N1−H1B···O4, 2.912(3) Å, and N1−H1C···O6, 2.905 (3) Å; Table 1). A small torsion angle of 8.952(134)° between N1−C15 and the line normal to the best plane also indicates that it is easy to form a pendulum movement and create the structural polarization (Figure S3).[9]

Although it is difficult to obtain clear single-crystal structures at high-temperature state 1 (**HTPS-1**) because of the high level of disorder, we have gotten the basic unit cell parameters of **HTPS-1** (high-temperature p4p data files for compounds 1 and 2); the crystal structure of **HTPS-1** still crystallizes in the orthorhombic crystal system but with a centrosymmetric orthorhombic space group *Cmcm* and a nonpolar point group *mmm* corresponding to a paraelectric phase. According to the Curie symmetry principle, the space group in the low-temperature phase is a subgroup of the one in the high-temperature phase (primary phase).[3,4] In our case, $Pca2_1$ is a subgroup of *Cmcm*.

As proven by our previous works, this crown ether clathrate can be regarded as a rotator−stator in which the protonated cyclohexylammonium cation is a rotator and the 18-crown-6 is a stator.[9,10] When the temperature is lower than $T_c$ (393 K), the cyclohexylammonium cation is frozen in alignment in the same direction; thus, the electric doublets cannot cancel each other along the *c* direction because of the oriented arrangement from the dipoles of the Hcha cations (Figures 1c and S4). This kind of polarization mechanism has been found previously in TGS (triglycine sulfate). When the temperature is higher than 393 K, the pendulum motion of the cyclohexyl ammonium is activated. At such high temperatures, the cyclohexylammonium is highly disordered like a rotator unit, and this low-temperature arrangement is broken, leading to its lying in a more highly symmetric and more disordered situation with the dipolar moment canceled. This molecular thermal motion mode is confirmed by the *c*-axis dielectric measurements given below.

**3.2. Powder X-ray Diffraction.** Because of the seriously disordered state of compounds **1** and **2** at high temperatures, we cannot obtain their clear crystal structures. To further

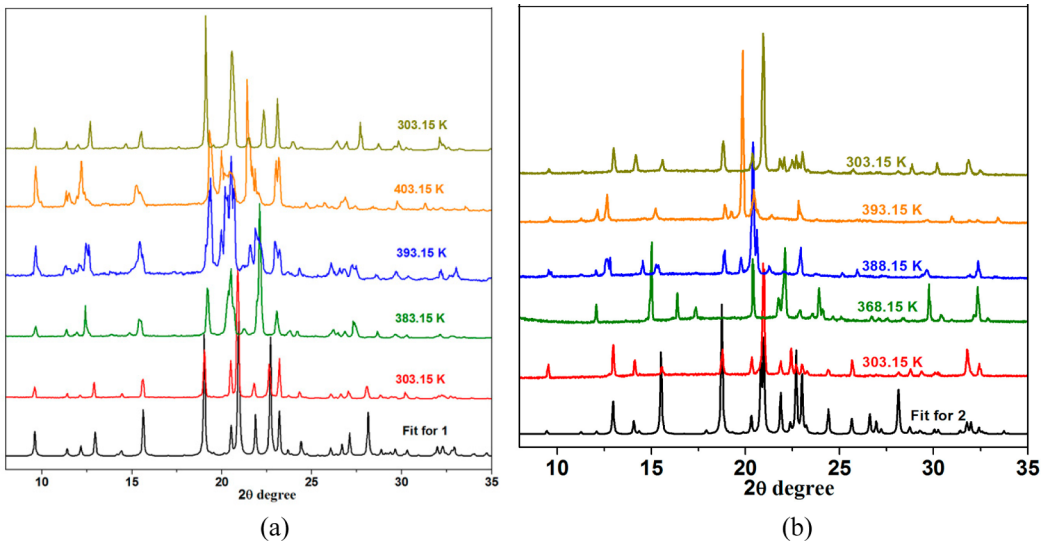


**Figure 2.** Powder XRD patterns of (a) **1** and (b) **2** as-synthesized samples at different temperatures by grinding.



DOI: 10.1021/jacs.5b08061
J. Am. Chem. Soc. 2015, 137, 13345−13351

confirm the phase transitions of both compounds, we carried out their variable-temperature PXRD measurements. As illustrated in Figure 2a, for compound **1** in the temperature range of 303−393 K, there is no obvious change in the diffraction peaks except for a little variety on their intensity. Then, at 403 K, above $T_c$, as shown by the yellow line, the sharp decrease of the number of diffraction peaks such as those at 12.2, 14.8, 21.5, 22.7, and 28.3° suggests a structural transition from low to high symmetry. When cooling back to 303 K, the PXRD pattern returns to that recorded for the starting materials again.[12] Similar to **1**, within the temperature range of 303−388 K, there are no changes in the diffraction peaks for compound **2** (Figure 2b). Although the temperature is beyond 393 K, the similar sharp decrease of the number of diffraction peaks such as those at 14.8, 20.7, 29.5, and 32.3° shows a structural phase transition from low to high symmetry. If the temperature was cooled back to 303 K, then its PXRD pattern agreed well with that recorded at starting materials.[12] As expected, these results show obvious phase-transitions temperatures consistent with their DSC measurement discussed in below.

As known, the question of how to make clear the microstructural changes in such a high-temperature phase transition is really a new challenge when X-ray single-crystal diffraction is not available. Because these reversible structural transitions are possibly caused by the order−disorder of certain local groups of host−guest molecules, which can be also reflected by their Raman bands, we recorded the temperature evolutions of the Raman bands in the total region 100−3200 $cm^{-1}$ (Figures 3 and S5). As can be seen, there is no obvious

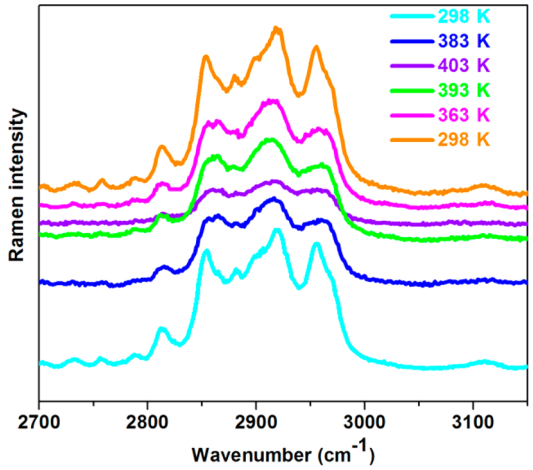


**Figure 3.** Temperature evolutions of Raman bands related with the N−H region for **1**.

change before the region of 2600 $cm^{-1}$ in the heating−cooling cycle of compound **1**, indicating that the basic framework of a 18-crown-6 ether is relatively stable and not very sensitive to the temperature in the structural phase transition; however, there are some clear distinctions in the range of 2600−3000 $cm^{-1}$. Vibrational frequencies in this region could be due to the coupling of the stretching modes of N−H group vibrations. At the initial temperature of 298 K, there are four continuous sharp peaks (2825, 2870, 2925, and 2958 $cm^{-1}$) in the pattern for **1**. With the increase of the temperature (recorded as 298 and 383 K), these peaks become broader and smoother. When the temperature is higher than the transition temperature, $T_c$ = 397 K, as shown with purple line (403 K), these sharp peaks almost develop into a horizontal line. In contrast, these modes become gradually sharp and narrow with the lowering of the temperature (recorded as 393, 363, and 298 K, respectively). Until the temperature is returned to 298 K, these patterns (yellow line) repeat those recorded with the starting materials, indicating a completely reversible structural phase-transition behavior.[12] These reversible changes in Raman spectra further confirmed the order−disorder orientation of cyclohexyl ammonium in phase transition. At high temperature, the cyclohexylammonium groups are disordered and have symmetric stretching modes corresponding to the paraelectric phase. Thus, the peaks are smooth and broadened; when they lie at a low temperature, all the cyclohexylammonium groups are ordered and have asymmetric stretching modes, showing the peaks as sharp and narrow, corresponding to the ferroelectric phase.

For compound **2**, variable-temperature Raman spectra patterns (Figures S6 and S7) reveal a similar reversible phase transition within the temperature range of 303−405 K. These obvious reversible changes in both compounds in the regions range of 2600−3000 $cm^{-1}$ further verify the coupling of the stretching modes of N−H group vibrations in both compounds.

**3.3. Thermal Properties.** Another effective way to detect whether this compound shows a reversible phase transition triggered by temperature is to perform DSC measurement to see if there is significant existence of heat anomaly happening during the heating and cooling process. As illustrated in Figure 4a, the crystalline sample of **1** undergoes a single phase transition at approximately $T_c$ = 390 K on a heating and cooling cycle, uncovering an endothermic peak at 397 K and an exothermic peak at 385 K. Furthermore, the sharp peaks and a reversible phase transition with a large, 12 K thermal hysteresis clearly reveal that it is a typical first-order phase transition. To further investigate thermal anomaly behavior of **1**, we calculated its entropy changes ($\Delta S$) for the phase transitions. By calculus methods, we estimated the entropy changes to be 15.79 $J\cdot mol^{-1}\cdot K^{-1}$ on the heating process (Supporting Information). According to the Boltzmann equation $\Delta S = R \ln N$, where $R$ is the gas constant and $N$ is the ratio of possible configurations, the calculated $N$ is approximately 6.67 around $T_{C1}$. Similarly, the calculated entropy changes ($\Delta S$) and $N$ values on account of the cooling process are estimated to be 15.05 $J\cdot mol^{-1}\cdot K^{-1}$ and 6.03, respectively, for the phase transition around $T_{C2} \approx$ 385 K.[10]

Similar to that of compound **1**, for compound **2** in the heating-cycle process, the entropy changes ($\Delta S$) are calculated to be 28.05 $J\cdot mol^{-1}\cdot K^{-1}$; thus, we can infer the value of $N$ is 29.19. However, in the cooling-cycle process, the corresponding entropy changes ($\Delta S$) and $N$ values are estimated to be 25.23 $J\cdot mol^{-1}\cdot K^{-1}$ and 20.78, respectively, for the phase transition around $T_{C2} \approx$ 377 K (Figure 4b). In comparison with complex **1**, complex **2** has much larger entropy changes ($\Delta S$) and $N$ values than those of **1**. This extremely large value of $N$ suggests that compound **2** undergoes much severer structural transformations around $T_{C1}$ and $T_{C2}$ characterized by typical order−disorder phase transitions. Moreover, to detect the thermal stabilities, thermogravimetric analyses for both compounds were carried out in the range of 293−1173 K. The TGA curves depicted in Figure S8 indicate that the decomposition temperatures of compounds **1** and **2** are 480 and 500 K, respectively, far beyond the phase-transition temperatures (397 and 390 K, respectively).


DOI: 10.1021/jacs.5b08061
J. Am. Chem. Soc. 2015, 137, 13345−13351

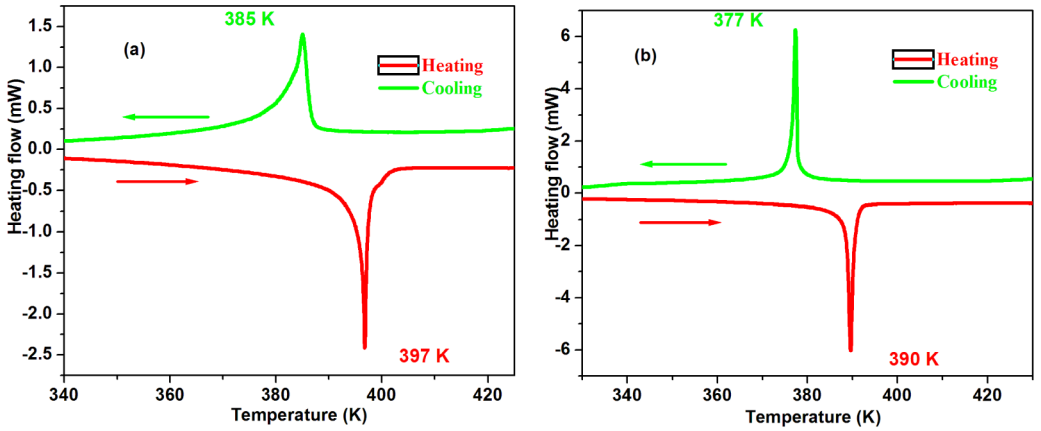


(a) (b)

**Figure 4.** DSC curves for (a) **1** and (b) **2** in the heating−cooling cycle.

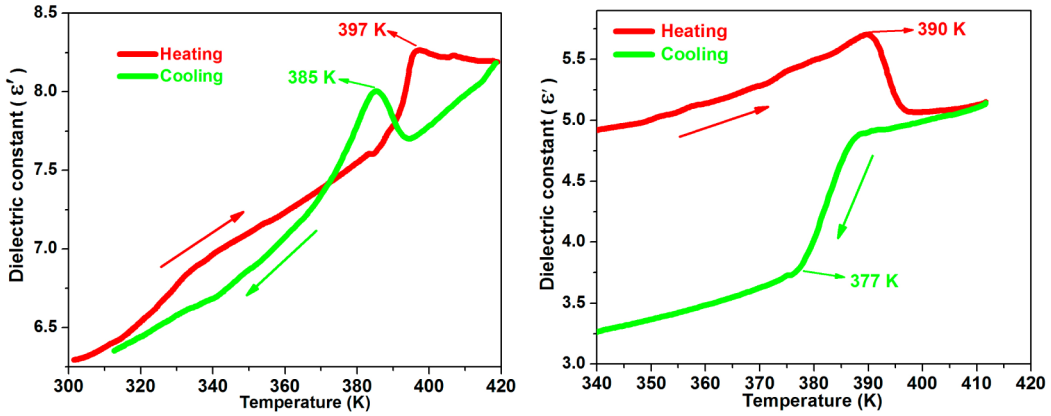


**Figure 5.** Dielectric properties for (a) **1** and (b) **2** measured as a function of temperature under a frequency of 10 kHz.

In recent years, three typical crown ether clathrates ferroelectrics with phase transitions have been reported, such as 4-methoxyanilinium tetrafluoroborate-18-crown-6 ($[C_7H_{10}NO\text{-}(18\text{-crown-}6)]^+[BF_4]$ , **3**), (DIPA) [18-crown-6]$BF_4$, **4**, and $Ca(NO_3)_2$(15-crown-5), **5**.[7,8] However, there are a lot of distinct differences between them and the title compounds. On the one hand, all the reported crown ether clathrate ferroelectrics have low phase-transition temperatures such as 127 K for **3**, 120 K for **4**, and 205 K for **5**; on the other hand, most of them display the second-order ferroelectric phase transition. As is known, the second-order ferroelectric phase transition often features a slight temperature hysteresis and a small entropy change ($\Delta S$) and $N$ values, whereas the first-order ferroelectric phase transition has the opposite characteristics.[4,7,8] The high ferroelectric phase transition and spontaneous polarization of title compounds are promising, with a wide application in modern materials.

**3.4. Dielectric Properties.** A variety of physical properties, e.g., the dielectric constant, usually display distinct changes in the vicinity of the phase transition. Measurements of the dielectric constant's dependence on temperature for **1** and **2** were recorded on single-crystal samples in a heating−cooling cycle mode, under the applied electric field $E$ parallel to the $a$ axis (at room temperature) with a frequency of 10 kHz. As illustrated in Figure 5a, for compound **1**, the real part of the dielectric constant increases slowly with the increase of temperature, and then the temperature is closed to 397 K, it exhibits a prominent increase with a maximum value 8.35. Subsequently, the dielectric constant descended very slowly and then remained at about 8.10 before 420 K. When the temperature falls down from 420 K, the real part of dielectric constant goes down slowly; then, in the vicinity of 385 K, there is another quick increase accompanied by an abrupt and narrow peak. Although the temperature is lower than 385 K, there is not any distinct change in the graph.

Similar to that of compound **1**, as shown in Figure 5b, the real part of the dielectric constant of **2** exhibits a clear increase with an abrupt slope at around 390 K in the heating-cycle mode, the maximum value is about 5.75 corresponding to a high dielectric state, then the dielectric constant goes down quickly with the increasing of temperature. The real part of dielectric constant remains at about 4.88 at temperatures higher than 393 K. Different from **1**, there is no obvious sharp peak observed in the cooling-cycle mode of **2**; however, the dielectric constant displays a remarkable steplike change at around 377 K (green line in Figure 5b). When the temperature is higher than 382 K, the dielectric constant stay above 4.80, whereas when the temperature is lower than 377 K, the dielectric constant remains in the low dielectric state (below 3.72). To our knowledge, these steplike changes of dielectric constant are always a feature of structural phase transition that have been reported.[1,4,7,8]

As we expected, the curves of dielectric constants for both compounds obtained in the heating−cooling modes match well



DOI: 10.1021/jacs.5b08061
J. Am. Chem. Soc. 2015, 137, 13345−13351

with those of heat anomaly behavior (DSC) heating−cooling, further confirming their reversible phase-transition behaviors.

**3.5. Ferroelectric Hysteresis Loop.** The ferroelectric natures of **1** and **2** have been directly verified by hysteresis measurements of the electric polarization ($P$) versus electric field ($E$). Both compounds share similar features except for a little difference on their polarization ($P_s$) and phase-transition temperature. Here we detail the dielectric hysteresis loops of **1** from 298 to 403 K. As shown in Figure 6, the $P-E$ loops under

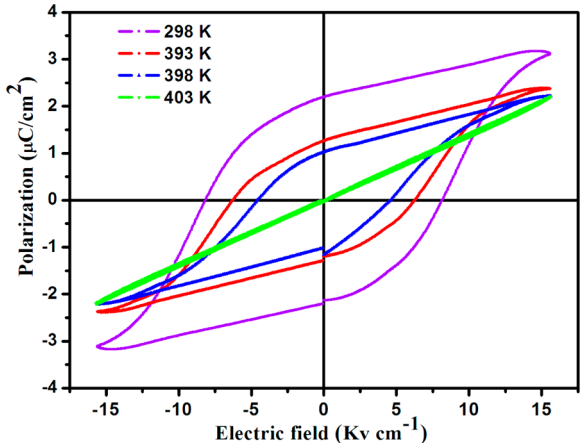


**Figure 6.** Electric hysteresis loops of **1** determined along the $c$ axis at different temperatures. The measured frequency is 50 Hz.

the electric field of a triangle waveform were recorded along the $c$ axis. When the sample was tested at 298 and 393 K, the curves display similar perfect ferroelectric loops without large change; then, with the increasing temperature, the loops gradually become smaller. After the temperature is above 397 K, it becomes a canted line, indicating that the ferroelectric−paraelectric phase transition has been completed. Specifically, when we used the max pulse width of 8 ms and applied field of 16 kV/cm at 298 K, the currently optimized $P_s$ reaches 3.27 $\mu$C/cm$^2$ for **1**. For compound **2** (Figure S9), the dielectric hysteresis loops show a larger polarization intensity than that of **1**; the optimized spontaneous polarization ($P_s$) reaches 3.78 $\mu$C/cm$^2$ at 298 K. This magnitude is much larger than that of most reported molecular ferroelectrics, i.e., ([$C_7H_{10}$NO-(18-crown-6)]$^+$[$BF_4$], (0.54 $\mu$C/cm$^2$) and (DIPA)[18-crown-6)]$BF_4$ (0.3 MC/cm$^2$),[7,8] and much closer to that of typical ferroelectrics such as KDP and Rochelle salt.[13]

## 4. CONCLUSIONS

We have successfully explored two new ferroelectrics, ([Hcha-(18-crown-6)]$^+$ [$BF_4$]$^-$ and ([Hcha-(18-crown-6)]$^+$ [$ClO_4$]$^-$. Totally different from most previously reported molecular ferroelectrics, crown ether clathrates **1** and **2** display unusual high-temperature reversible phase-transition behaviors, large spontaneous polarization, and temperature hysteresis. This research explores a new method to design and seek the new type of ferroelectrics as well as broadens their application in modern materials.

## ■ ASSOCIATED CONTENT

### Supporting Information

The Supporting Information is available free of charge on the ACS Publications website at DOI: 10.1021/jacs.5b08061.

Figures S1−S9 and calculation of $\Delta S$ and $N$ for compound **1**. (PDF)

Crystallographic information file for compound **1**. (CIF)

Crystallographic information file for compound **2**. (CIF)

High-temperature p4p data file containing basic unit-cell parameters of compound **1**. (DOC)

High-temperature p4p data file containing basic unit-cell parameters of compound **2**. (DOC)

## ■ AUTHOR INFORMATION

### Corresponding Author

*tangyunzhi75@163.com

### Notes

The authors declare no competing financial interest.

## ■ ACKNOWLEDGMENTS

We sincerely thank Prof. Ren-Gen Xiong for his kind help. We also thank Prof. Heng-Yun Ye for polishing the manuscript carefully. We are grateful for the financial support from the National Natural Science Foundation of China (grant nos. 21261009, 21461010, and 21471070), Young Scientist Foundation of Jiangxi Province and Jiangxi Province Science and Technology Support Program (20133BBE50020), and the Patent Sustentation Fund from Jiangxi Province (3203304622).

## ■ REFERENCES

(1) (a) Horiuchi, S.; Tokunaga, Y.; Giovannetti, G.; Picozzi, S.; Itoh, H.; Shimano, R.; Kumai, R.; Tokura, T. *Nature* **2010**, *463*, 789. (b) Fu, D.-W.; Cai, H.-L.; Liu, Y.-M.; Ye, Q.; Zhang, W.; Zhang, Y.; Chen, X.-Y.; Giovannetti, G.; Capone, M.; Li, J.-Y.; Xiong, R.-G. *Science* **2013**, *339*, 425. (c) Ye, H.-Y.; Fu, D.-W.; Zhang, Y.; Zhang, W.; Xiong, R.-G.; Huang, S. P. D. *J. Am. Chem. Soc.* **2009**, *131*, 42. (d) Zhang, W.; Chen, L.-Z.; Xiong, R.-G.; Nakamura, T.; Huang, S. P. D. *J. Am. Chem. Soc.* **2009**, *131*, 12544.

(2) (a) Sun, Z.-H.; Chen, T.-L.; Luo, J.-H.; Hong, M.-C. *Angew. Chem., Int. Ed.* **2012**, *51*, 3871. (b) Xu, G.-C.; Ma, X.-M.; Zhang, L.; Wang, Z.-M.; Gao, S. *J. Am. Chem. Soc.* **2010**, *132*, 9588. (c) Hang, T.; Fu, D.-W.; Ye, Q.; Ye, H.-Y.; Xiong, R.-G.; Huang, S. P. D. *Cryst. Growth Des.* **2009**, *9*, 2054. (d) Li, M.-Y.; Kurmoo, M.; Wang, Z. M.; Gao, S. *Chem.—Asian J.* **2011**, *6*, 3084.

(3) (a) Lines, M. E.; Glass, A. M. *Principles and Applications of Ferroelectrics and Related Materials*; Oxford University Press, U. K.,1977;. (b) Jona, F.; Shirane, G. *Ferroelectric Crystals*; Pergamon Press: Oxford, U.K., 1962. (c) Lines, M. E.; Glass, A. M. *Principles and Applications of Ferroelectrics and Related Materials*; Oxford University Press, New York, 2001.

(4) (a) Zhang, W.; Xiong, R.-G. *Chem. Rev.* **2012**, *112*, 1163. (b) Sun, Z.-H.; Luo, J.-H.; Zhang, S.-Q.; Ji, C.-M.; Zhou, L.; Li, S.-H.; Deng, F.; Hong, M.-C. *Adv. Mater.* **2013**, *25*, 4159.

(5) (a) Schulze, G. *Z. Angew. Math. Mech.* **1962**, *43*, 512. (b) Ahn, C. H.; Rabe, K. M.; Triscone, J. M. *Science* **2004**, *303*, 488. (c) Haertling, G. H. *J. Am. Ceram. Soc.* **1999**, *82*, 797. (d) Scott, J. F. *Science* **2007**, *315*, 954.

(6) (a) Horiuchi, S.; Tokura, Y. *Nat. Mater.* **2008**, *7*, 357. (b) Zhang, W.; Xiong, R.-G. *Chem. Rev.* **2012**, *112*, 1163. (c) Tang, Y.-Z.; Zhou, M.; Huang, J.; Tan, Y.-H.; Wu, J.-S.; Wen, H. R. *Inorg. Chem.* **2013**, *52*, 1679. (d) Tang, Y.-Z.; Yu, Y.-M.; Tan, Y.-H.; Wu, J.-S.; Xiong, J.-B.; Wen, H.-R. *Dalton Trans.* **2013**, *42*, 10106. (e) Tang, Y.-Z.; Xiong, J.-B.; Gao, J.-X.; Tan, Y.-H.; Xu, Q.; Wen, H.-R. *Inorg. Chem.* **2015**, *54*, 5462.

(7) (a) Zhang, W.; Ye, H.-Y.; Cai, H.-L.; Ge, J.-Z.; Xiong, R.-G.; Huang, S. P. D. *J. Am. Chem. Soc.* **2010**, *132*, 7300. (b) Zhang, W.; Ye, H.-Y.; Xiong, R.-G. *Coord. Chem. Rev.* **2009**, *253*, 2980.

(8) (a) Zhang, W.; Xiong, R.-G.; Huang, S. P. D. *J. Am. Chem. Soc.* **2008**, *130*, 10468. (b) Ye, Q.; Song, Y.-M.; Wang, G.-X.; Chen, K.; Fu,



DOI: 10.1021/jacs.5b08061
J. Am. Chem. Soc. 2015, 137, 13345−13351

D.-W.; Hong Chan, P. W.; Zhu, J.-S.; Huang, S. P. D.; Xiong, R.-G. *J. Am. Chem. Soc.* **2006**, *128*, 6554.
(9) (a) Fu, D.-W.; Zhang, W.; Cai, H.-L.; Zhang, Y.; Ge, J.-Z.; Xiong, R.-G.; Huang, S.-D. *J. Am. Chem. Soc.* **2011**, *133*, 12780. (b) Ye, H.-Y.; Li, S.-H.; Zhang, Y.; Zhou, L.; Deng, F.; Xiong, R.-G. *J. Am. Chem. Soc.* **2014**, *136*, 10033. (c) Ge, J.-Z.; Fu, X.-Q.; Hang, T.; Ye, Q.; Xiong, R.-G. *Cryst. Growth Des.* **2010**, *10*, 3632.
(10) (a) Ye, H.-Y.; Zhang, Y.; Fu, D.-W.; Xiong, R.-G. *Angew. Chem.* **2014**, *126*, 6842. (b) Zhang, Y.; Ye, H.-Y.; Fu, D.-W.; Xiong, R.-G. *Angew. Chem., Int. Ed.* **2014**, *53*, 2114.
(11) (a) Sheldrick, G. M. *SHELXS-97, Programs zur Lösung von Kristallstrukturen*; University of Grttingen: Grttingen, Germany, 1997. (b) Sheldrick, G. M. *SHELXS-97, Program for X-ray Crystal Structure Refinement*; University of Grttingen: Grttingen, Germany, 1997.
(12) (a) Swain, D.; Bhadram, V. S.; Chowdhury, P.; Narayana, C. *J. Phys. Chem. A* **2012**, *116*, 223. (b) Tang, R.; Li, Y.; Li, N.; Han, D.; Li, H.; Zhao, Y.-S.; Gao, C.-X.; Zhu, P.; Wang, X. *J. Phys. Chem. C* **2014**, *118*, 10560. (c) Mączka, M.; Ciupa, A.; Gągor, A.; Sieradzki, A.; Pikul, A.; Macalik, B.; Drozd, M. *Inorg. Chem.* **2014**, *53*, 5260.
(13) Abdel-Jawad, M.; Terasaki, I.; Sasaki, T.; Yoneyama, N.; Kobayashi, N.; Uesu, Y.; Hotta, C. *Phys. Rev. B: Condens. Matter Mater. Phys.* **2010**, *82*, 125119.



DOI: 10.1021/jacs.5b08061
*J. Am. Chem. Soc.* 2015, 137, 13345−13351